Best Practices for Predicting Acoustics of a Single Rotor Using the NASA RVLT Conceptual Design Toolchain

Lauren Weist
Aerospace Engineer

Natasha Schatzman
Aerospace Engineer

Dorsa Shirazi
Aerospace Engineer

Aeromechanics Office
NASA Ames Research Center
Moffett Field, CA, USA

ABSTRACT

To facilitate the development of the Urban Air Mobility (UAM) market, the NASA Revolutionary Vertical Lift Technology Project has created the Conceptual Design Toolchain, a suite of tools developed and/or selected to assist rotorcraft designers in all stages of rotorcraft design. Of particular interest to the UAM noise community are the following two steps in this toolchain: comprehensive analysis and acoustic prediction. Since the UAM application is relatively new, there is a need for a systematic study on how best to utilize these codes. To this end, the current study documents best practices for using the comprehensive analysis codes, CAMRAD II and CHARM, along with the acoustic code AARON. Two single rotors are considered: i) a simple rotor and ii) a rotor that is more representative of what UAM designers might use. Best practices are presented for the prediction of both tonal and broadband self-noise, along with the corresponding results. The goal is to provide conceptual designers the tools to conduct accurate noise prediction using the RVLT Conceptual Design Toolchain.

NOTATION

BL_T	Boundary layer trip setting
C_T	Coefficient of thrust
h	Trailing edge wedge thickness (m)
M_{AT}	Advancing tip Mach number
R	Blade radius (m)
t/c	Maximum thickness-to-chord ratio
$v_{ind,x}$	Induced velocity, + forward direction (m/s)
$v_{ind,y}$	Induced velocity, + right direction (m/s)
$v_{ind,z}$	Induced velocity, + up direction (m/s)
V_∞	Free stream velocity (m/s)
α_0	Zero-lift angle of attack (deg)
α_s	Shaft tilt (deg)
α_{eff}	Effective angle of attack (deg)
θ_0	Blade collective angle (deg)
θ_{TE}	Trailing edge wedge angle (deg)
μ	Advance ratio
σ	Solidity
ϕ	Observer elevation angle (deg)
ψ	Observer azimuth angle (deg)
Ω	Angular velocity (rad/s)

Presented at the Vertical Flight Society's 6th Decennial Aeromechanics Specialists' Conference, Santa Clara, CA, Feb. 6-8, 2024.

INTRODUCTION

The NASA Revolutionary Vertical Lift Technology (RVLT) Project aims to provide the U.S. Government, industry, and academia with cutting-edge rotorcraft tools and technologies. In particular, the RVLT Conceptual Design Toolchain ('the toolchain') was developed to evaluate the noise and performance of multirotor aircraft. This toolchain has many capabilities, including comprehensive analysis and acoustic prediction. Currently, the toolchain provides a choice of two industry codes for comprehensive analysis, while acoustic prediction is performed using US Government developed software. To assist in the transition of these codes to a wider audience, a study was conducted to develop best practices for conducting acoustic analysis coupled with these comprehensive analysis codes.

Comprehensive analysis in the toolchain can currently be performed using either the Comprehensive Analytical Model of Rotorcraft Aerodynamics and Dynamics II (CAMRAD II) (Ref. 1) or the Comprehensive Hierarchical Aeromechanics Rotorcraft Model (CHARM) (Ref. 2). Acoustic predictions are performed using the Aircraft NOise Prediction Program - Second Generation (ANOPP2) tool, Aeroacoustic ROtor Noise (AARON), and the Python wrapper pyaaron (Ref. 3). Each code has a user's manual, and several authors have published papers using the comprehensive analysis and acoustic portion of the toolchain to gain acoustic results. Some authors of note are Silva (Ref. 6), Kottapalli (Refs. 11, 12), and

Weist (Ref. 13). That being said, to date there is not a 'best practices' document for using these codes to conduct acoustic predictions.

These best practices are not a direct comparison between CAMRAD II and CHARM, but a study of how to produce noise prediction results with either code. These best practices are developed with a new or novice user in mind, and are aimed at reducing the time and effort required for a user to execute the toolchain for acoustic predictions.

This study covers the best practice development for two single rotors, selected with increasing complexity. The first rotor is a simple, isolated rotor developed by Leonard Lopes ('the Lopes rotor') (Ref. 4) and the second is the main rotor of a RVLT reference concept vehicle, the Quiet Single Main Rotor (QSMR) (Ref. 5). The Lopes rotor is a four-bladed main rotor with idealized airfoil sections, that is, airfoil tables that have a linear angle of attack with reduced sections and Mach number relations and no blade stall or moments. The QSMR is a more complex main rotor that contains blended SSC-A09 and VR-12 airfoils. To counteract main rotor torque, the QSMR utilizes a NOTAR configuration (not modeled in this work).

BACKGROUND

Rotorcraft acoustic prediction requires high-resolution blade loading and motion data in order to be accurate. For the toolchain, this blade loading is provided by comprehensive analysis codes. Comprehensive analysis codes are mid-fidelity tools, which compute blade information more quickly than CFD while still retaining moderate fidelity. Often, these codes are coupled with an acoustic prediction code to produce predictions of the acoustics of a given rotorcraft configuration.

RVLT Toolchain

The RVLT Conceptual Design Toolchain is a suite of codes used in the evaluation of noise and performance of rotary wing vehicles. Figure 1 details the complete toolchain, which contains multiple codes covering different areas of the conceptual design space. The work presented in this paper focuses on two areas of the toolchain: comprehensive analysis and acoustic prediction, shown in boxes 2 and 3 in Fig. 1.

The first of two comprehensive analysis codes is CAMRAD II, a mid-fidelity comprehensive analysis code developed by Johnson Aeronautics that simultaneously solves the rotorcraft dynamics and aerodynamics for trimmed and transient flight conditions. For the current acoustic predictions, lifting-line theory is used to model the aerodynamics of the blade (Ref. 1). The second comprehensive analysis code is CHARM. Developed by Continuum Dynamics, Inc., CHARM models rotorcraft dynamic and aerodynamics, is mid-fidelity, and uses the constant vorticity contour method to model the aerodynamics for acoustic predictions (Ref. 2). Both CAMRAD II and CHARM perform the same basic function, but the models and code architectures differ, which can lead to differences in the results.

For acoustics, the toolchain makes use of a NASA-developed acoustic prediction code suite. The foundation of this suite is ANOPP2, which consists of a framework, tools, and functional models used to compute noise. ANOPP2 includes,

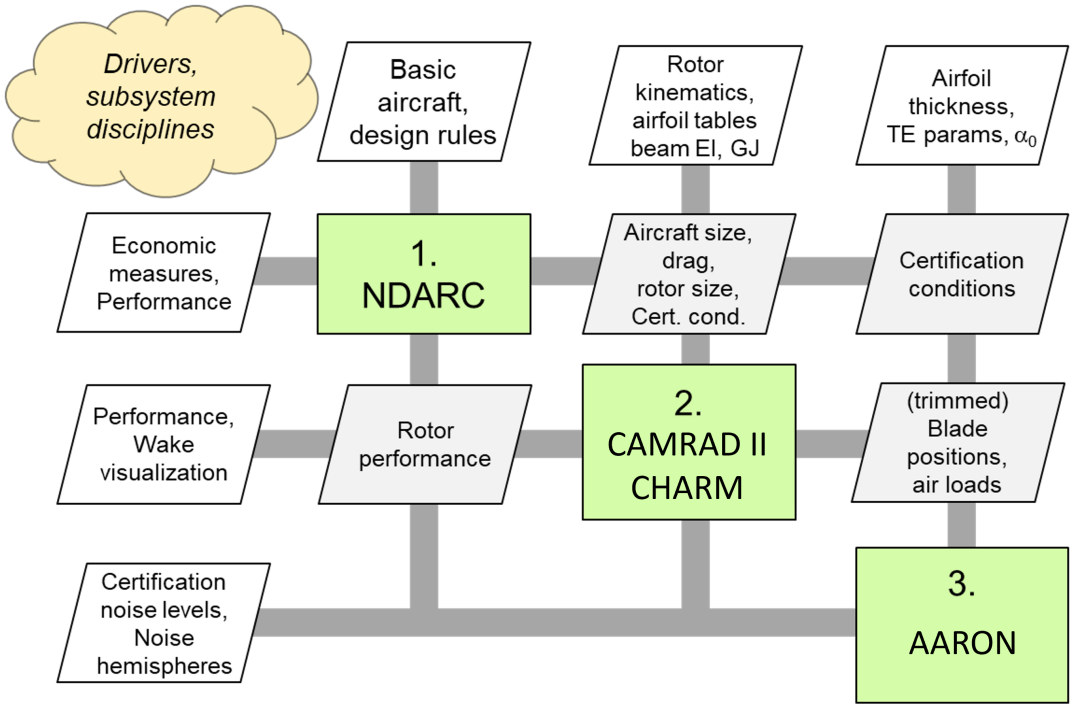

Figure 1. NASA RVLT Conceptual Design Toolchain workflow from Ref. 6.

among others, the integral formulation of the Ffowcs Williams and Hawkings equations, known as Farassat's Formulation 1A (F1A) (Ref. 7). Both the compact thickness and the compact loading version of F1A are used for this work. For broadband self-noise, the Brooks-Pope-Marcolini semi-empirical model is used (Ref. 8). The FORTRAN interface tool AARON, which is part of the ANOPP2 system, is used to make rotorcraft specific calculations.

To assist in the interfacing of these tools, two Python codes, RCOTools and pyaaron, were used. RCOTools is a set of Python utilities and wrappers for the toolchain that is designed to facilitate data transfer and is capable of reading, modifying, and writing files (Ref. 9). pyaaron, a Python tool developed by Doug Boyd at NASA Langley, uses RCOTools to automate the running of comprehensive analysis codes with AARON. pyaaron parses and executes the chosen comprehensive code and then feeds relevant information to AARON for ANOPP2. This code works for both CAMRAD II and CHARM, and adds several capabilities to AARON to enhance its usefulness to the toolchain.

Developing best practices

As the codes used by the toolchain are complicated in nature, and the way they interact with each other requires a specific practice, it was decided that a set of best practices needed to be developed to aid a user in choosing the correct (optimum) settings for these codes. One of the goals of this work is also to increase the standardization and ease of use of comprehensive analysis codes for acoustic prediction, and to make sure the information is available to a wide audience within academia, industry, and government.

These best practice investigations are not designed to compare the results of CAMRAD II and CHARM; instead, both codes are used to generate similar results to ensure correct settings are used. The goal of this work is not to identify a 'best code' but to instead provide the best practices when using either or both of these codes.

METHODS

In order to develop best practices for a wide range of possible rotorcraft models, a methodology of increasing complexity was adopted. The first configuration explored was a simple four-bladed main rotor with no twist or taper and idealized airfoil tables. This case was called the 'Lopes Rotor' as it was developed by Leonard Lopes at NASA Langley, who published simulation results for this rotor (Ref. 4). From there, the study moved on to the NASA RVLT reference vehicles, which are example eVTOL configurations that have publicly accessible designs for use by the rotorcraft community. This paper looks specifically at one reference vehicle, the Quiet Single Main Rotor (QSMR). For building either model in CAMRAD II or CHARM, starting with the closest available completed model is recommended. This is often a sample model provided with the comprehensive codes.

For both the Lopes rotor and the QSMR, the models were completed by modifying a sample case. This reduces the amount of knowledge a user needs in formatting and base model building, which decreases the time it takes to get a model running. This method also ensures that all parameters required for trim are accounted for, even if they won't be used in the acoustic analysis. Making the vehicle model as complete as possible will lead to more accurate acoustic results, even if components such as the fuselage or tail rotor aren't currently being considered directly in the acoustic analysis.

For each case, acoustic results were predicted for 21 observer locations. This study uses 8 in-plane (or azimuthal) and 13 out-of-plane (or elevation) observers that span from 0 to 360 degrees in-plane and 0 to -180 degrees out-of-plane, shown in Fig. 2. This series of observers can capture the maximum thickness noise, which occurs in line with the rotor disk, and the maximum loading noise, which occurs below the rotor. The current range of microphone locations also allows various broadband self-noise sources to be captured. Throughout this paper, a selection of microphones within this range that represent the results found will be shown.

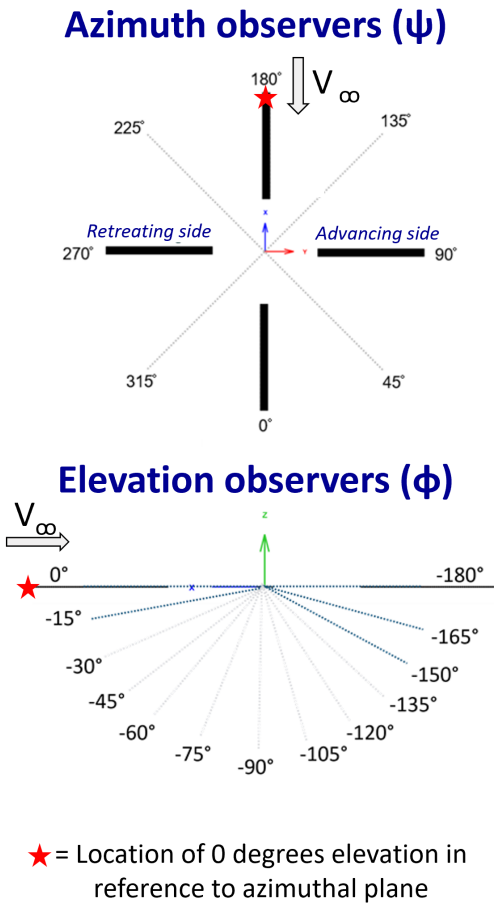

Figure 2. Hemisphere of observers used in AARON for both the Lopes rotor and the QSMR.

Rotor models

The first rotor analyzed, the 'Lopes rotor,' is a simple, hingeless, rigid, four-bladed isolated rotor with a constant chord and airfoil and no twist. The acoustics models for the Lopes rotor contain no tail rotor or fuselage. A rigid hub model was used to allow for collective only trim. Table 1 provides the rotor parameters and Fig. 3 shows a mock-up of the blades in OpenVSP. Twenty-one observers were used to completely capture the acoustic environment around the rotor, both in-plane and below the rotor.

Table 1. Lopes and QSMR rotor parameters. *Idealized airfoils are a modified NACA 0012 that has reduced angle of attack stations, and no stall or moments.

	Lopes rotor	QSMR
Number of Blades	4	3
Blade Radius (R)	10 m	5.04 m
Chord Length	0.5 m	0.756 m
Geometric solidity (σ)	0.06366	0.044
Angular Velocity (Ω)	23.69 rad/s	42.37 rad/s
Linear twist rate	0 deg/span	-12 deg/span
Airfoil sections	Idealized*	VR-12 & SSC-A09

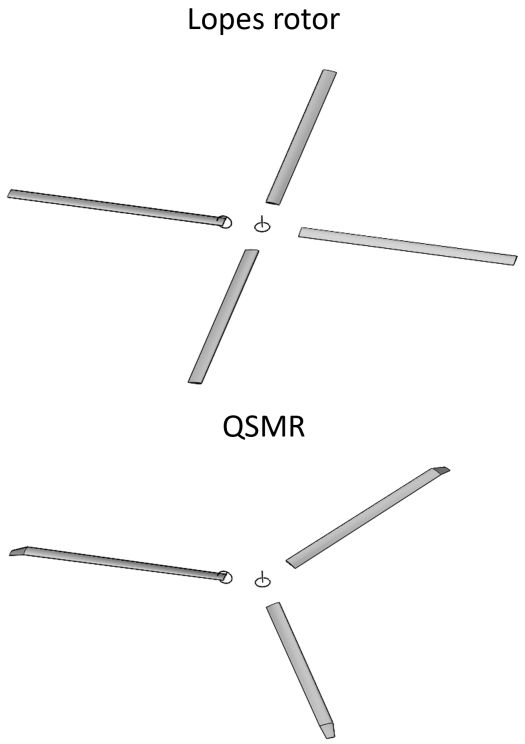

Figure 3. OpenVSP mock-ups of both the Lopes and QSMR rotors modeled in CAMRAD II and CHARM.

The second rotor used in this work is the main rotor of the QSMR RVLT reference vehicle. The 3-bladed rotor contains both twist, taper, and droop. Additionally, the QSMR contains varying airfoil sections, blending an inboard VR-12 airfoil to an SSC-A09 airfoil towards the tip at 0.94R. This rotor also uses a hinge model that allows for full blade motion, that being flap, lead-lag, and feathering. The QSMR rotor parameters are also shown in Table 1 and 3. The same observer sphere as the Lopes rotor was used. For the CHARM model, a tail rotor was also modeled to provide anti-torque in trim, although it was not processed for acoustics. In CAMRAD II, both a tail rotor and fuselage were modeled to account for vehicle weight to assist in trim, but were not included in the acoustic results.

BEST PRACTICES

As the two rotors were analyzed, a list of best practices was developed. For these best practices, results are shown for each use case to verify practices and give example results that a user should expect to produce. A selection of results are shown for the Lopes rotor and for the QSMR for each of the flight conditions considered.

Initial steps

The first step to conducting acoustic analysis in either CAMRAD II or CHARM is to configure the codes to generate acoustic outputs. For CAMRAD II, the sound sensor 'OPSND' must be turned on, and several aerodynamic sensors must be enabled to output the information required by AARON. Figure 16 in Appendix A outlines the various settings required to get proper outputs for AARON. It is recommended that a user put these settings into a .list file and include them in the CAMRAD II run. For CHARM, slightly fewer inputs are required in the main input file, the most important setting being 'NOISE.' Also in Appendix A, Fig. 17 shows the noise settings in CHARM used in this work. These settings allow for outputs to be properly formatted for use with AARON. Turning on these settings in both CAMRAD II and CHARM is the first step to conducting acoustic noise prediction with AARON.

Panel and azimuth resolution

There are several settings in both CAMRAD II and CHARM that must be set to specific values in order to get the codes to converge and produce valid acoustic results. The first to consider is the number of aerodynamic panels used in CAMRAD II and CHARM, which separate the blade into spanwise sections for calculation purposes. For CAMRAD II, the number of panels defines both the aerodynamic sections and wake sections; the panels need to be adequately spaced to prevent the sections from being too closely spaced in areas of complex flow, which could cause code failure. This is due to the way CAMRAD II is coded, as the program struggles when there is too many wake trailers in areas of complex flow. For

most rotors, though there are some exceptions such as rotors with low tip speeds, 15-25 aerodynamic panels is ideal as it captures adequate detail without causing convergence issues. In CHARM, the wing aerodynamic panels and wake sections are defined separately, and therefore do not need to be as carefully considered, although 50 aerodynamic panels are generally considered sufficient (CHARM only allows up to 100 panels).

Figure 4 shows the effect of different numbers of panels on loading noise for both CAMRAD II and CHARM for the QSMR model. For CHARM, the number of panels had very little effect on noise. The 25 panel case, shown in red, only showed a slight increase in noise likely due to insufficient panels. For CAMRAD II, the number of panels had a much larger effect on noise. The QSMR was run in CAMRAD II for 10, 20, 30, and 50 panels, with only the 10 and 20 panel cases converging. Even then, the 10 panel case, pictured in red, has a large amount of additional noise. Since the CAMRAD II manual states that 15-25 panels are recommended, these noise spikes can be attributed to having insufficient panels. This study was also conducted for the Lopes rotor, but as this was a very simple configuration, the cases converged without issue for each case and contained no variation in noise.

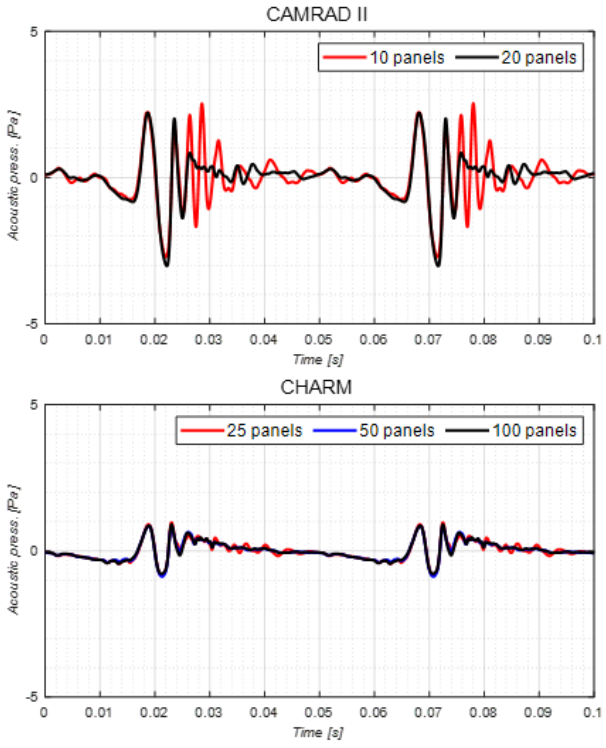

Figure 4. Loading noise acoustic pressure time history panel study for the QSMR forward flight free wake with both CAMRAD II and CHARM (V_{inf} =53.9 m/s, $\frac{C_T}{\sigma}$ = 0.07, μ = 0.25, α_s = -3°, θ_0 = 4°).

For CHARM, additional consideration should be taken for how the segments are partitioned. CAMRAD II automatically partitions the blade to account for airfoil and chord changes, while in CHARM it can either be generated with a blade geometry input file Utility or calculated manually. For this paper, the geometry of the Lopes/QSMR rotor used in CHARM was manually generated. The partitioning locations, root twist, and twist per section span were completed in a spreadsheet, starting with the number of spanwise sections being used for the blade. Then the total desired twist on the blade can be divided between each segment to get the twist increments used. To follow convention, a root twist should be added so that the 75% span location on the blade has a twist of 0. This calculation can then be used as the CHARM input for twist. The final verification required is that the number and size of segments aligns with when the airfoil type or chord size changes, that is, that a segment begins just as a change in chord or airfoil begins. For example, the QSMR has an airfoil change at 0.94R, and so a segment should start at the 0.94R location to capture this.

The second setting to consider is the number of azimuthal stations. As stated previously, acoustics requires high resolution data, as there is high frequency noise that needs high azimuthal resolution to be captured. At least 360 azimuthal stations per revolution are recommended for CAMRAD II. For CHARM, it is recommended for either 240 or 360 stations to be used. Using too high of an azimuthal resolution in CHARM can lead to numerical noise in the result, so sometimes an even lower azimuthal resolution is required. It is recommended to start with 240 and reduce the resolution if the results contain unsteady peaks to eliminate numerical noise as a possible cause. It can sometimes take a few tries to find the correct balance between high enough resolution to capture high-frequency noise but low enough resolution to eliminate numerical errors. This resolution cannot be applied in the initial calculation for CHARM and is not recommended in CAMRAD II; therefore, it must instead be calculated at the end of a CAMRAD II or CHARM run. For CHARM, this is done via a method called 'reconstruction,' while in CAMRAD II this process is called 'post-trim.' The initial calculation in either code should be a factor of 10 smaller than the final calculation to ensure no numerical noise is introduced.

CAMRAD II and CHARM model settings

One of the major sources of error when modeling in both CAMRAD II and CHARM is not accounting for differences in the inputs. As CAMRAD II and CHARM have differing underlying models, it is often the case that similar (or the same) variables require different inputs. One such difference is that CHARM uses a negative Fourier series (NACA convention) for flapping angles, while CAMRAD II uses the more common positive Fourier series. That means that β_{1c} and β_{1s} will have different signs between CAMRAD II and CHARM.

CAMRAD II and CHARM also use different representations of thrust. CHARM trims to C_T while CAMRAD II trims to $\frac{C_T}{\sigma}$. This means that while a user may be trimming both codes to the same value, C_T must be input for CHARM, while $\frac{C_T}{\sigma}$ must be input for CAMRAD II. If this is not done the codes

will trim to different thrust values and the acoustic results could differ dramatically.

In CHARM, the number of revolutions (NREV) also needs to be considered. NREV defines the number of blade revolutions in the trim solution. Having a high NREV value, such as 200, ensures that a stable trim is achieved for loading predictions. Having too few revolutions will lead to an unstable result, and could affect the loading noise results.

Rotor model complexity

Another best practice is to minimize the complexity of the initial model and then increase the complexity in steps. For example, this study began with the Lopes rotor in a 'simple wake,' discussed later in this paper, with rigid, hingeless blades and an idealized NACA 0012 airfoils in hover (reduced angle of attack stations and 0 moments). This allows a user to verify that the rotor model is correct while reducing the errors from the flight condition and airfoil. Reducing the number of variables makes it easier to identify where a case may be failing. This is when a user may, for example, find issues in rotation direction, shaft angle, rotor orientation, hub model, or trim settings.

Once the simple case is working, then one can begin increasing complexity. The first thing to do is implement a more realistic airfoil. For the case of the Lopes rotor, this airfoil was a simple idealized airfoil. But for the QSMR, the airfoils used were a blended SSC-A09 and VR-12 airfoil section, which is much more complicated than an idealized airfoil. Introducing a complicated airfoil can be a challenge, as airfoil data is not always available, and can be difficult to verify for the applications of interest (UAM configurations).

The next step, once the models are performing as expected, is to move on to forward flight. Often this will illuminate issues in trim and blade loading, as forward flight contains an asymmetrical loading environment and is more dependent on rotor configuration. This should still be done using the simple wake model initially, as using the simple wake is a good last step to verify the basic model before moving into free wake. The total tonal noise of the simple wake forward flight case for both the Lopes rotor and QSMR are shown in Figs. 5 and 6, respectively. The acoustic environment for the simple wake is very periodic and smooth in nature, as any irregularities from wake-interaction have yet to be introduced. This result

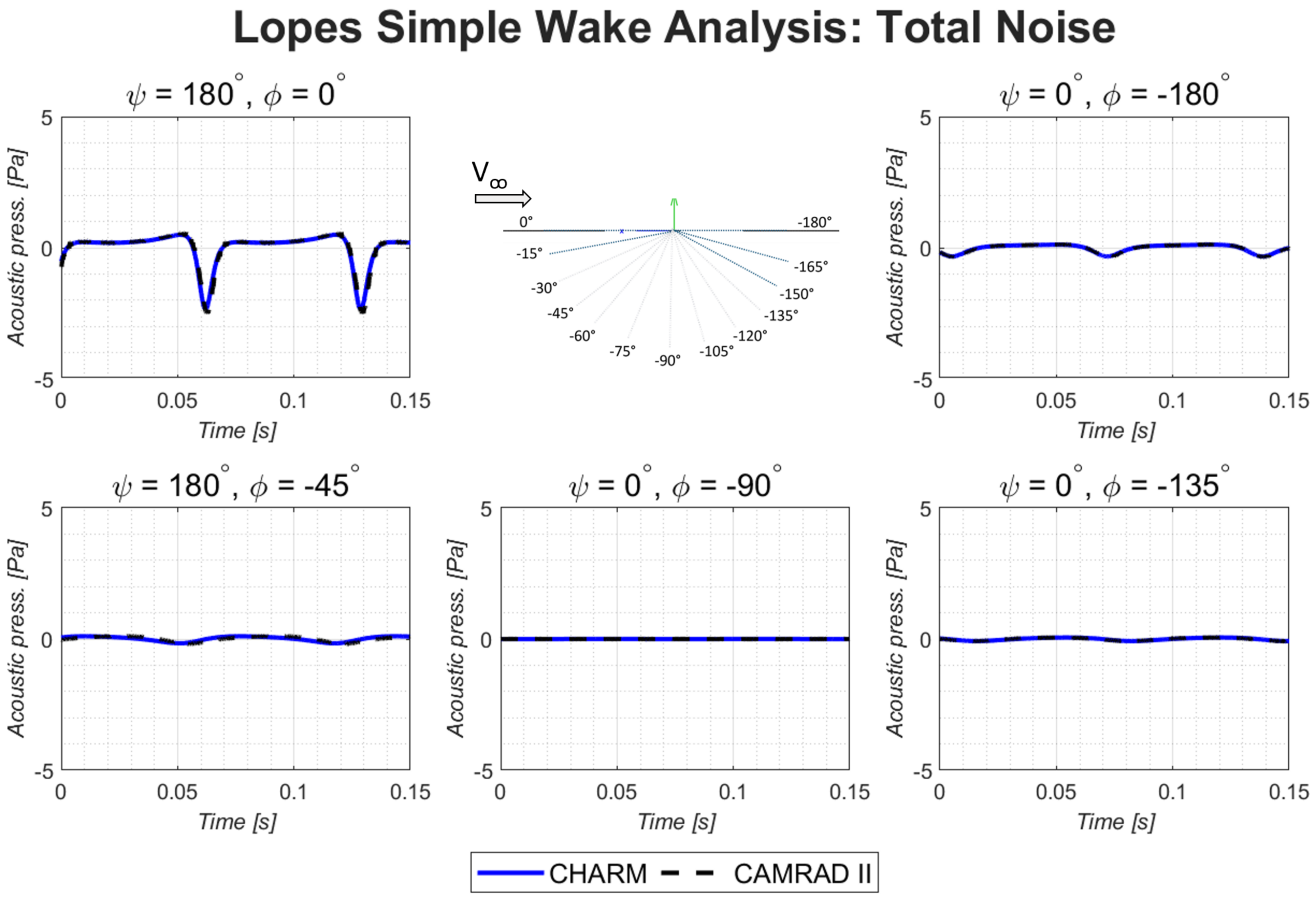

Figure 5. Total noise (thickness + loading) in CAMRAD II and CHARM using AARON for the Lopes rotor in forward flight with a simple wake model (V_{inf} =33.5 m/s, $\frac{C_T}{\sigma}$ = 0.001, μ = 0.14, α_s = 5°, θ_0 = -1°).

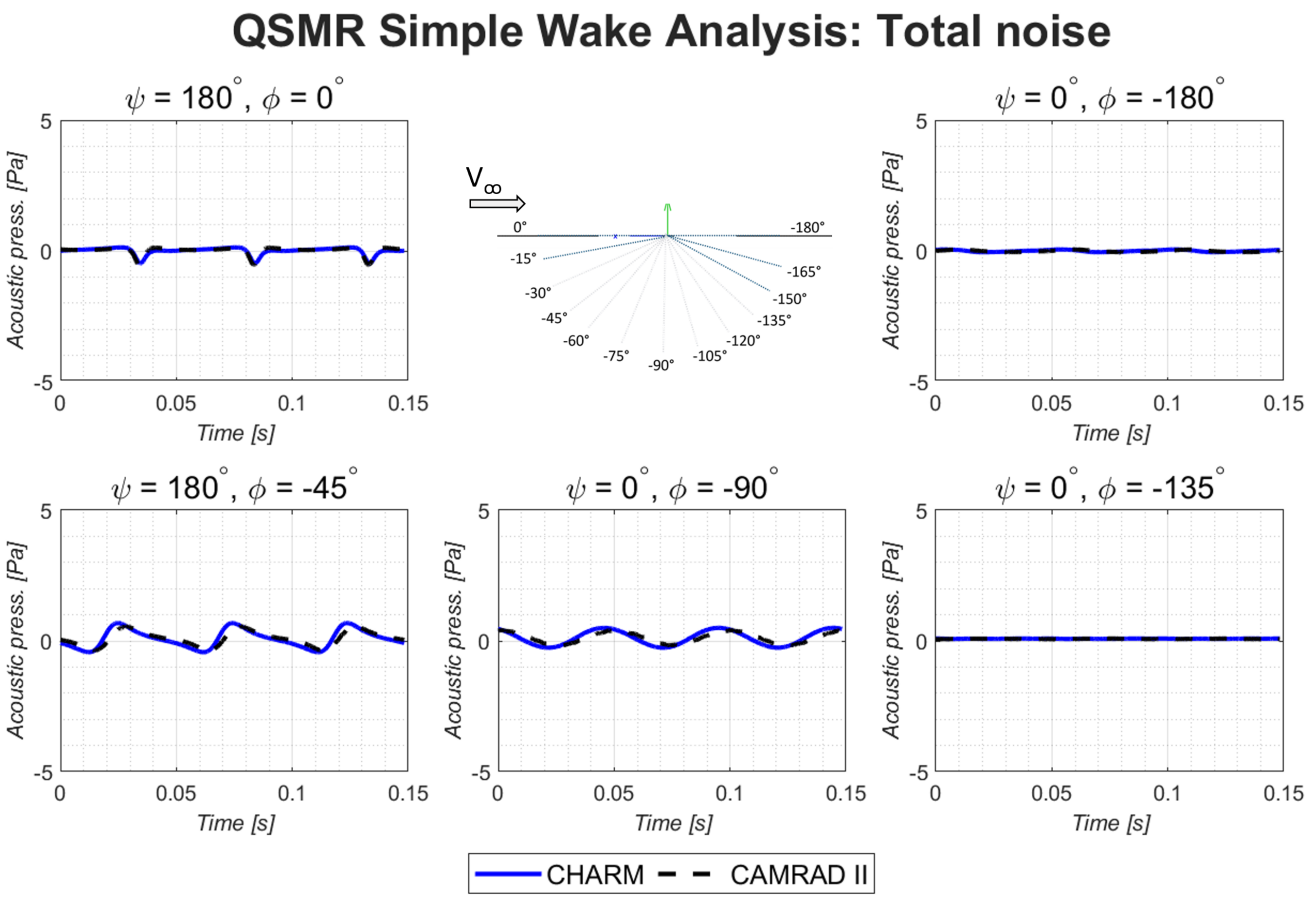

Figure 6. Total noise (thickness + loading) in CAMRAD II and CHARM using AARON for the QSMR in forward flight with a simple wake model (V_{inf} =53.9 m/s, $\frac{C_T}{\sigma}$ = 0.08, μ = 0.25, α_s = -3°, θ_0 = 4°).

mainly captures the noise from the air displacement (thickness noise) and the noise from the forces on the blade (loading noise) which all function on a per revolution basis. Thickness noise is often, but not always, dominant in-plane of the rotor, and is seen in periodic pressure dips as each blade passes the observer. Loading noise is dominant out-of-plane, and is seen as small hills in the acoustic signature.

Wake settings

Once the user is satisfied with both the hover and forward flight simple wake model, it is then suggested to increase the fidelity of the model. Both CAMRAD II and CHARM have models for simple wake, rigid wake, and free wake (Ref. 10). A 'simple wake' uses uniform inflow to calculate the wake-induced velocities. The uniform inflow is a quasi-static representation of the wake from momentum theory. This model only accounts for linear variations over the rotor disk and is, therefore, the easiest to model and least computationally expensive. The next step in wake complexity is a rigid wake, which models the wake as a skewed helix with no wake contractions or vortex distortions. This can also be done with a prescribed wake, which is similar to a rigid wake. As this accounts for some wake interactions, it is used as an intermediate step between the simple wake and the more complex free wake. Finally, the highest fidelity wake for this study, the free wake, is used. The free wake calculates the distorted wake geometry including the induced velocities of all vortex elements on all others, and therefore accounts for wake contractions and vortex distortions. The free wake calculates more accurate blade loading compared to the uniform and rigid wake models, which is required for acoustic predictions. When used in both hover and forward flight, this methodology analyzes cases with increasing accuracy and increasing complexity.

The ideal wake progression of simple wake to free wake is shown in Fig. 7. It is useful to use the rigid wake as a model verification stage, as the inputs are not as complicated as those of the free wake, but it is closer to the accuracy and complication level of the free wake. In this stage, the acoustics should follow the smooth curves seen in the simple wake case, but may contain some variation caused by rotor-wake interactions. Once the rigid wake is operating correctly, then the free wake can be approached.

The free wake is the highest fidelity model offered by most comprehensive analysis codes without coupling with CFD,

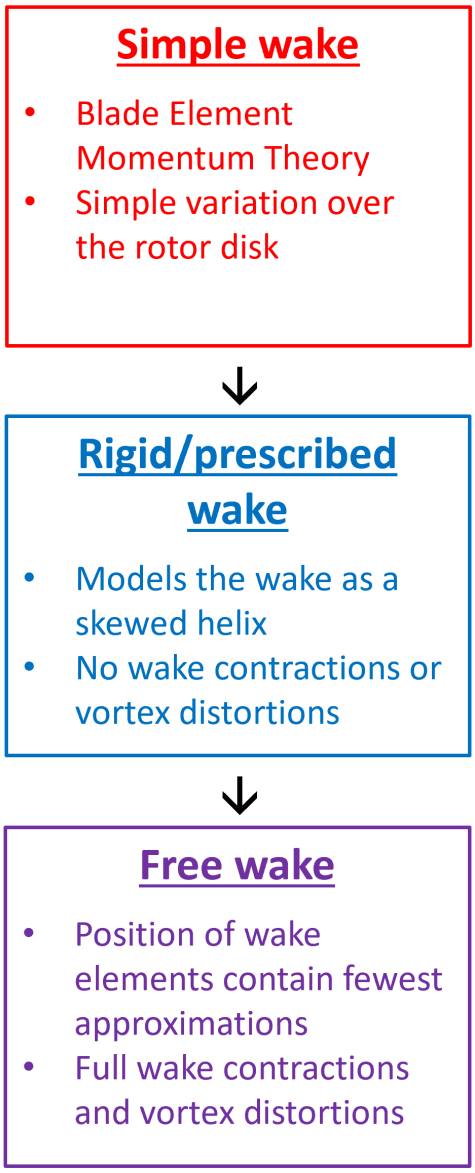

Figure 7. The progression of wake modeling for CAMRAD II and CHARM cases.

and therefore requires more information to be read in. The acoustic results for the free wake could contain much more rotor-wake interactions, and could have less smooth noise profiles. This is not always the case, but for some configurations, such as low speed forward flight rotors, the wake can have a large effect. It is important to work with a free wake when using comprehensive analysis to produce acoustic results, as wake-interaction noise, such as that caused by blade-vortex-interaction, can cause highly tonal, and in some cases highly annoying, noise signatures. Capturing these signatures is necessary to understanding the acoustic environment of the rotor being studied.

Broadband self-noise parameters

AARON uses the Brooks-Pope-Marcolini (BPM) semi-empirical model for broadband self-noise prediction (Ref. 8). This model is rather low fidelity, and uses a combination of user-supplied inputs and comprehensive code outputs. In the current study, a code was written to automatically generate the user inputs for the BPM model for various rotor configurations, showcased in this section. Additionally, predictions of broadband self-noise were completed for both the Lopes rotor and the QSMR using a free wake in forward flight.

The BPM model requires several user-supplied inputs to conduct broadband self-noise predictions. These parameters are included in the pyaaron namelist file and are a function of fractional rotor radius. The inputs are as follows: trailing edge wedge angle (θ_{TE}), trailing edge wedge thickness (h), maximum thickness-to-chord ratio (t/c), boundary layer trip setting (BL_T), and zero-lift angle of attack (α_0). These inputs, with the exception of boundary layer trip setting, are functions of the airfoil geometry. Figure 8 displays the BPM parameters that are from airfoil geometry. Trailing edge wedge angle is the angle between the upper and lower airfoil surfaces, and requires a user to project a line between the upper and lower surfaces, as airfoils often have a blunted trailing edge that is ignored in the BPM model. This can be done by identifying two points on the upper and lower surface of trailing edge, using those points to project two lines, then solving for the angle between those two lines. The trailing edge wedge thickness is the height of the end of the trailing edge wedge, and can be pulled from the geometry of the airfoil. Maximum thickness-to-chord ratio can also be pulled from the airfoil geometry, as it is the height of the thickest point of the airfoil divided by the chord length.

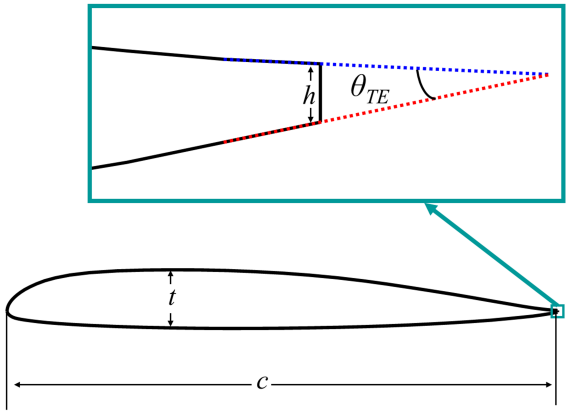

Figure 8. Airfoil geometry inputs for BPM model shown on an example airfoil section.

The non-geometric inputs required by pyaaron are zero-lift angle of attack and boundary layer trip setting. The zero-lift angle of attack, while also determined from the airfoil, is not found in the airfoil geometry. Instead, it is the location in the

airfoil tables where the airfoil angle of attack is generating 0 coefficient of lift. It is recommended to write a code that takes the Mach number at the given radial station, goes to that corresponding Mach number in the airfoil tables, finds the location where $C_L = 0$, and interpolates the corresponding angle of attack, which is then used as a BPM input. Due to changing Mach number along the span of the blade, the zero lift angle of attack changes for each radial station. Boundary layer trip setting, on the other hand, tells BPM whether to use the equation for a tripped boundary layer. This equation determines the thickness of the boundary layer at the trailing edge and is used to predict broadband self-noise from a turbulent trailing edge boundary layer, and can be turned on if a user desires to consider that parameter.

To better understand the contribution of each input to the pyaaron/AARON BPM model, a parameter variation study was performed for the QSMR in forward flight using the free wake model. Variations were made to the 'baseline' case (Case 1), which has the correct inputs for the BPM model for the QSMR. These inputs are listed in Table 3 in Appendix B. Then, six cases were created where in each case one broadband self-noise parameter was set to zero to view that parameter's effect on the BPM model. Table 2 lists each case and the parameter that was changed.

Table 2. QSMR broadband self-noise parameter study cases.

Case	Change from baseline
1	Baseline
2	$t/c = 0$
3	$\alpha_0 = 0$
4	$h = 0$
5	$\theta_{TE} = 0$
6	$BL_T = 1$
7	t/c, α_0, h, $\theta_{TE} = 0$; $BL_T = 1$

Results from the broadband self-noise parameter study on the QSMR in forward flight with a free wake are shown in Fig. 9 for cases 1 through 7. Total broadband self-noise was plotted from 0 Hz to 20,000 Hz for both CAMRAD II (outlined symbols) and CHARM (solid symbols). Most variations cause at least a minor change in broadband self-noise. Setting thickness-to-chord and zero-lift angle of attack to 0 (Case 2 and 3) lead to a change in SPL under 6,000 Hz, both settings inducing the same changes in noise. Changing trailing edge wedge thickness and angle (Cases 4 and 5) lead to a change in high frequency noise above 6,000 Hz. Finally, changing boundary layer trip setting (Case 6) lead to a change in SPL across the whole spectra.Therefore, it can be concluded that while each broadband self-noise parameter contributes to a different broadband self-noise source, each is important in understanding the total broadband self-noise environment of a rotor. If all these settings are turned off (or set to 1 in the case of boundary layer trip setting), as in Case 7, BPM still outputs broadband self-noise as BPM also relies on other additional parameters produced by the comprehensive codes, discussed as follows.

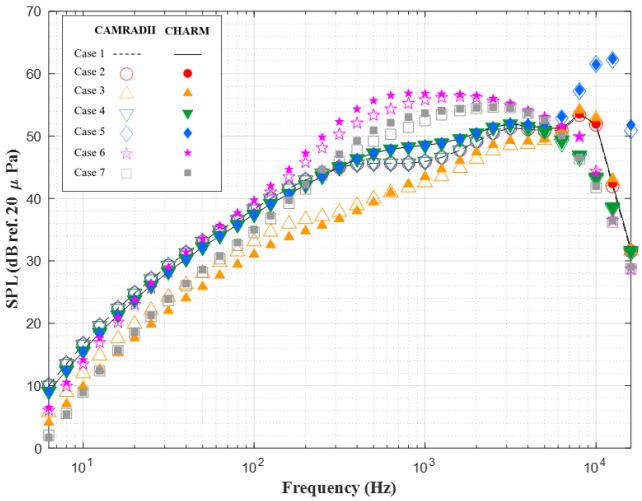

Figure 9. BPM parameter study for QSMR in forward flight free wake for cases 1 through 7 for total broadband self-noise (V_{inf} =53.9 m/s, $\frac{C_T}{\sigma}$ = 0.07, μ = 0.25, α_s = -3°, θ_0 = 4°).

Outside of user inputs, BPM also uses the output of effective angle of attack (α_{eff}) and induced velocity (V_{ind}) from either CAMRAD II or CHARM. These values provide BPM with information about inflow and blade lift. A user can look at these values via disk plots produced by pyaaron, which are a projection of the rotor disk over one rotation of one blade. As all blades are geometrically the same, these plots can be expected to be the same for each blade. Figure 10 shows the effective angle of attack and induced velocity disk plots for the QSMR in forward flight with a free wake for both CAMRAD II and CHARM. These values were used by the BPM model in both the parameter study and the final results to gain information about the aerodynamic environment for broadband self-noise prediction.

These disk plots can also be used as a comparison of the loading environments of CAMRAD II and CHARM. While both codes produce very similar plots, it is interesting to note that CAMRAD II has lines of increased loading along the span of the rotor disk that are rougher in nature, compared to the smooth lines of increased loading in CHARM. Additionally, CAMRAD II has a lower effective angle of attack on the retreating side of the rotor, shown in dark blue, as compared to CHARM. These differences can be attributed to the differences in azimuthal resolution and differences in the inflow model calculation method, as CHARM uses the constant vorticity contour method and CAMRAD II uses lifting line. Regardless, these differences may lead to slight variation in the broadband prediction, which is to be expected.

Figures 11 and 12 show the final BPM results spectra for both the Lopes rotor and QSMR, respectively. Both plots use the free wake forward flight model for each vehicle, and show both component noise sources and total noise sources. Results

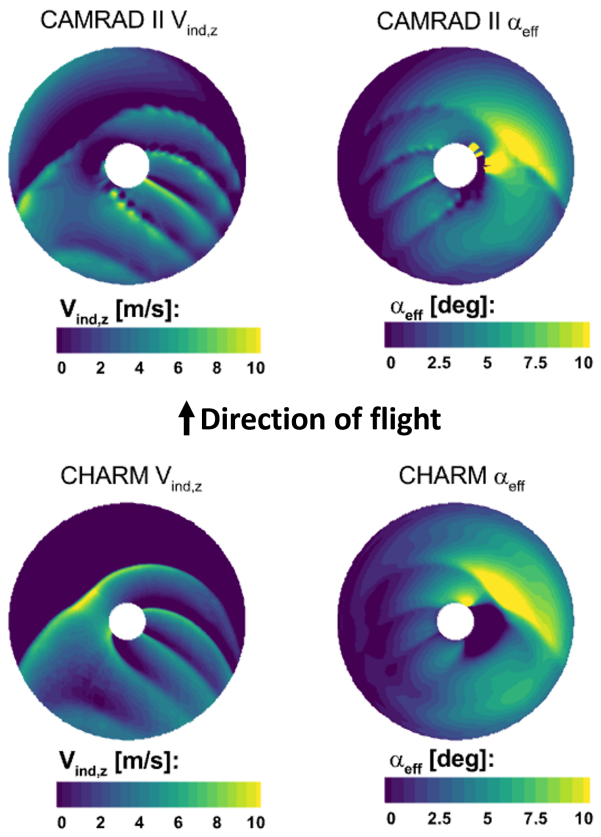

Figure 10. QSMR free wake forward flight disk plots for vertical induced velocity and effective angle of attack. Plots contain one revolution of one blade (V_{inf} =53.9 m/s, $\frac{C_T}{\sigma}$ = 0.07, μ = 0.25, α_s = -3°, θ_0 = 4°).

are plotted for both CAMRAD II and CHARM in a range of 0 to 20,000 Hz.

The Lopes rotor broadband self-noise results (Fig. 11) show a nearly exact match between CAMRAD II and CHARM, and have a maximum of 60 dB at 3,500 Hz. Looking at the noise components, the largest sources of broadband self-noise are pressure side and suction side sources. These sources are caused by the turbulent boundary layer on both the top (suction side) and the bottom (pressure side) of the airfoil. These results imply that the Lopes airfoil has a turbulent boundary layer around the whole blade, leading towards a high broadband self-noise.

Broadband self-noise results for the QSMR, Fig. 12, also show a close match between CAMRAD II and CHARM, with only slight variations of less than 1 dB in almost all terms. The peak broadband self-noise for the QSMR is at 53 dB and 9,000 Hz, and is dominated by both pressure side, suction side, and bluntness noise. Pressure and suction noise are caused by the same sources as those in the Lopes rotor, while bluntness noise is caused by a blunted trailing edge leading to vortex shedding. While this is an additional broadband self-noise source when compared to the Lopes rotor, the QSMR is

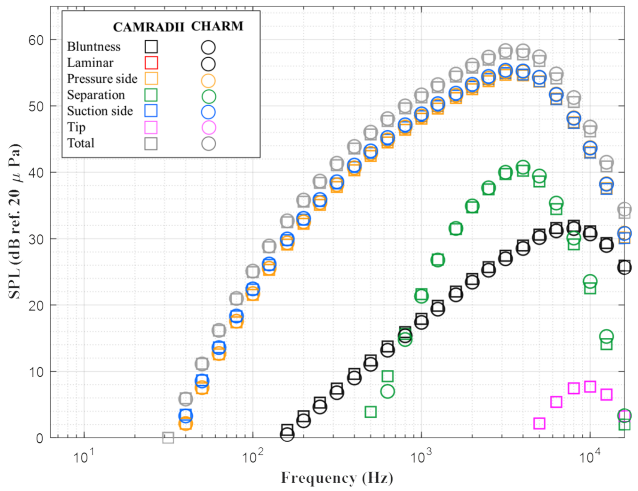

Figure 11. Lopes rotor free-wake in forward flight broadband self-noise predictions for CAMRAD II and CHARM (V_{inf} =33.5 m/s, $\frac{C_T}{\sigma}$ = 0.001, μ = 0.14, α_s = 5°, θ_0 = -1°).

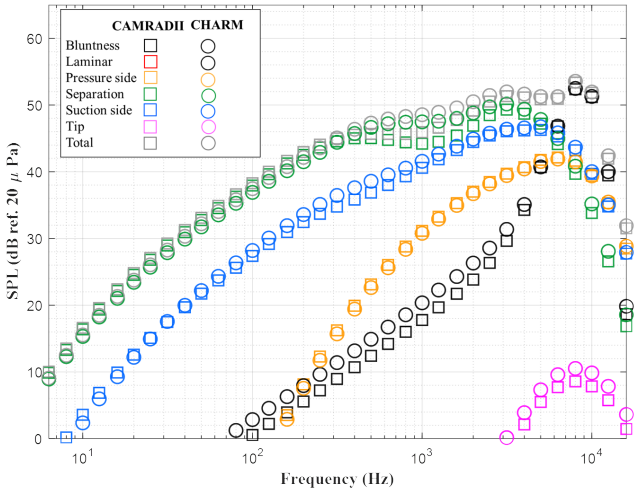

Figure 12. QSMR free-wake in forward flight broadband self-noise predictions for CAMRAD II and CHARM (V_{inf} =53.9 m/s, $\frac{C_T}{\sigma}$ = 0.07, μ = 0.25, α_s = -3°, θ_0 = 4°).

still quieter by 7 dB at the peak.

Debugging tools

Another methodology that is important to use when running these codes for acoustic prediction with AARON is to utilize metadata. Metadata is an output setting in AARON that produces TecPlot formatted files containing plots of all the internal parameters from an AARON run. Using metadata, a user can look in depth at what AARON is calculating and identify issues with the model. For this work, the z loading and z induced velocity were the most helpful debugging parameters. For loading noise, these two variables are the major inputs; therefore, differences in blade loading or induced velocity will be reflected in the acoustic results. By comparing

CAMRAD II and CHARM metadata side by side, one can see differences and where they are located along the blade.

Figure 13 shows the metadata comparison for the QSMR free wake z loading. These plots make it easy to see where possible differences in loading noise are coming from. Metadata calculations cover slightly more than one revolution of data, as metadata is produced for the entire calculation time from source to observer. These results are periodic in nature, so although there is more than one revolution displayed, the data simply begins to repeat itself. Analyzing metadata and identifying differences can aid in the identification of areas of further study. For example, in Fig. 13, there are loading differences towards the tip of the blade, seen as a yellow line of loading for CAMRAD II and a light green line in CHARM on the outside of the curves. This difference means there is likely some differences in the blade tip of the two models, either geometrically or in the tip loss factor. Another difference that can be seen is the differences in wake interaction magnitudes. Curved lines across the length of the blade are likely caused by blade-wake interactions of some kind, and can lead to high loading noise spikes. Since there are differences between these two plots, it is likely there are differences in the wake models between CAMRAD II and CHARM that have not entirely been resolved. By analyzing metadata in this manner and combining the metadata with a knowledge of the rotorcraft loading environment, understanding of the acoustic results due to blade loading can be gained.

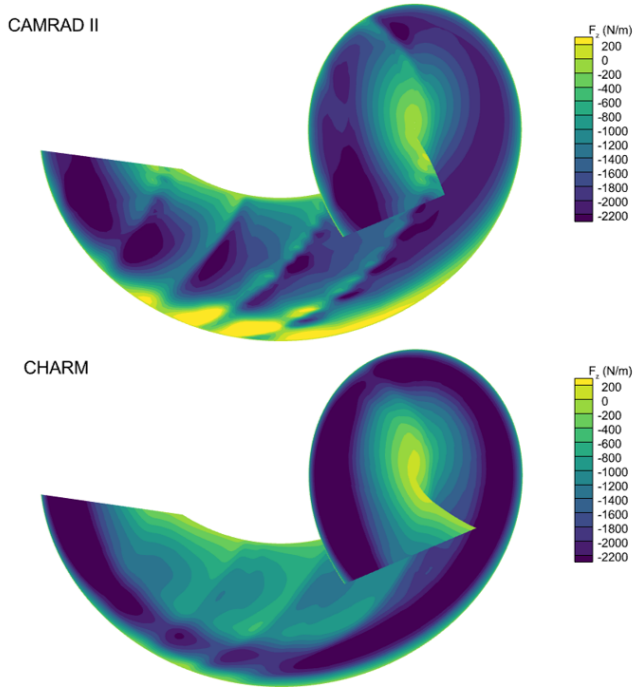

Figure 13. QSMR forward flight free wake, single blade z loading metadata for CAMRAD II and CHARM (V_{inf} =53.9 m/s, $\frac{C_T}{\sigma}$ = 0.07, μ = 0.25, α_s = -3°, θ_0 = 4°).

There are a variety of metadata parameters produced by AARON, and by looking through them, a user can identify areas where the solution looks off, such as having a plot of 0's, and therefore gain information as to where a solution may be going wrong. The disk plots shown in Fig. 10 are also useful for debugging, and can be used very similarly to the Metadata.

CAMRAD II AND CHARM FREE WAKE RESULTS

This section highlights the final comparison between the acoustic results for both CAMRAD II and CHARM. Final results are considered achieved when the rotor has been modeled in a trimmed, free wake state. It cannot be expected for the acoustic results of both CAMRAD II and CHARM to be exactly the same, as the methods of wake modeling are different, which can lead to differences in loading noise. Thickness noise is expected to match, as this comes from blade geometry. Broadband self-noise, calculated via the Brooks-Pope-Marcolini model, is expected to match as well. Additionally, with increasing complexity comes increasing reasons why the codes may not match, as both the trim and wake models differ between the two codes. CHARM uses a Constant Vorticity Contour free wake method, which utilizes a vortex lattice method to determine blade forces and moments, which then influence the noise (Ref. 2). CAMRAD II, on the other hand, uses the 'Johnson method,' which uses wake elements to calculate a vortex line, which has the equivalent velocity as a vortex sheet element (Ref. 1). This is then combined with the lifting line method to gain the forces and moments on the blade. As these two codes use different models and are implemented differently, there is going to be some differences in trim, blade loading, and acoustics. Therefore, one should not expect exact matches if comparing the two codes.

As broadband self-noise results were already shown in a previous section, this section focuses on total tonal noise. Figures 14 and 15 show the acoustic pressure time histories for the Lopes rotor and QSMR for two in-plane (in front and behind) and three out-of-plane (45 deg down in front, directly below, and 45 deg down behind) microphones. The two in-plane microphones display mostly thickness noise, while the three out-of-plane microphones contain mostly loading noise, due to the directivity of rotorcraft noise sources.

When comparing the results between the Lopes rotor and the QSMR, several key differences are apparent. The first difference is that the Lopes rotor has a much higher thickness noise than the QSMR, but a much lower loading noise. The thickness noise is due to the Lopes rotor having a thick, symmetric airfoil section, while the QSMR has an airfoil that has been optimized for low noise. Loading noise, on the other hand, is much higher for the QSMR than it is for the Lopes rotor. This can be attributed to the differences in the loading environment between the two rotors. The Lopes rotor has a lower flight speed and a $\frac{C_T}{\sigma}$ of 0.001 as compared to the QSMR's 0.07. This much slower and lower loading environment produces less loading noise, leading towards the Lopes rotor being quieter in this flight condition.

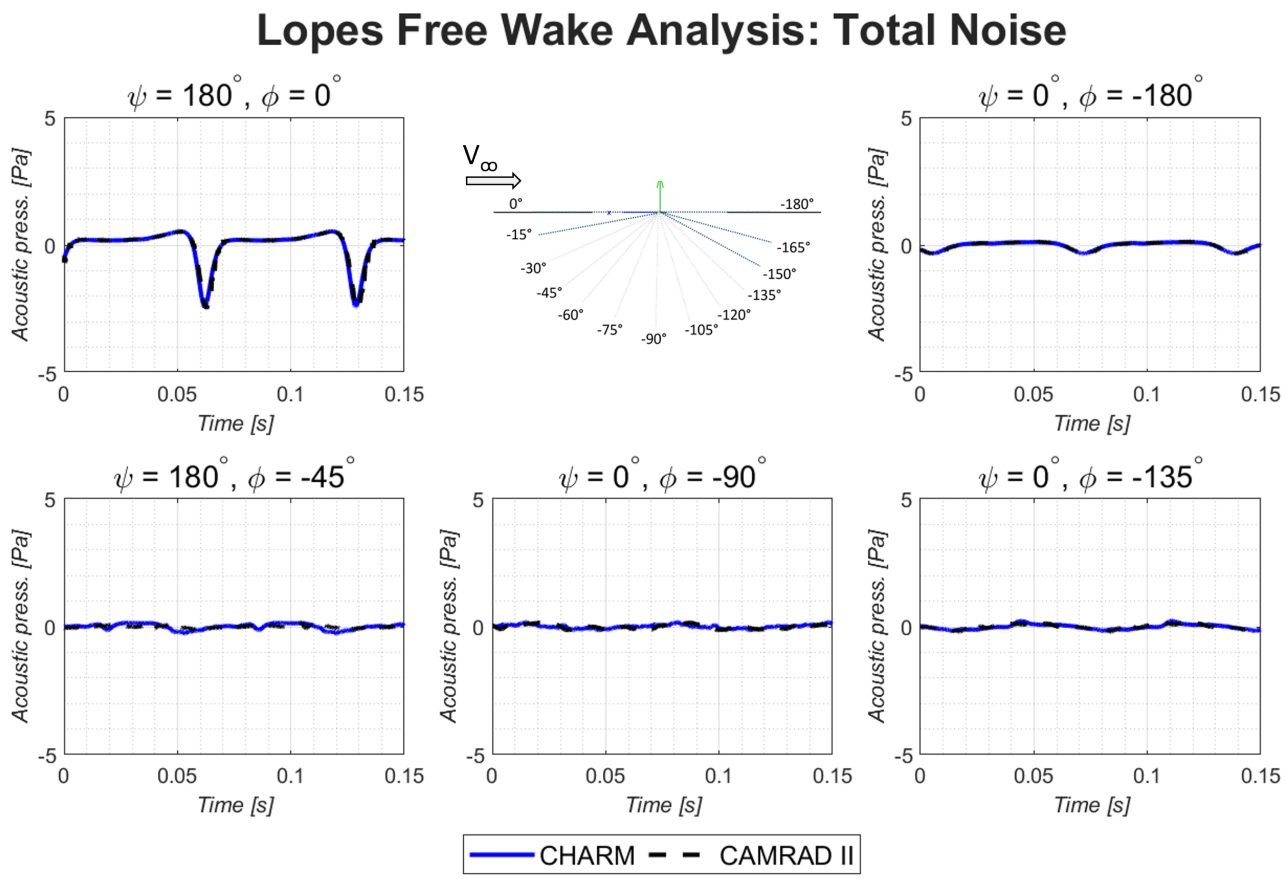

Figure 14. Total noise (thickness + loading) in CAMRAD II and CHARM using AARON for the Lopes rotor in forward flight with a free wake model (V_{inf} =33.5 m/s, $\frac{C_T}{\sigma}$ = 0.001, μ = 0.14, α_s = 5°, θ_0 = -1°).

Additionally, there are large differences between CAMRAD II and CHARM for the QSMR, which is not seen in the Lopes rotor.The main contributor of the Lopes rotor getting a good match is the low loading environment and relatively simple configuration. As the QSMR has a more complex loading environment and configuration, there are more areas where the differences between CAMRAD II and CHARM won't match. It can be expected to get the same mean noise environment, but getting an exact match would be difficult without experimental data to fine-tune the models. Regardless, the mean loading noise is captured with both codes, and the thickness noise is an exact match, providing users of these codes with a good understanding of the acoustic environment of these rotorcraft.

CONCLUSIONS

Best practices were developed for acoustic predictions using the acoustics code AARON with the comprehensive analysis codes CAMRAD II and CHARM as a part of the NASA RVLT Conceptual Design Toolchain. Two main rotors were shown: the Lopes rotor and the QSMR. The best practices are summarized as follows:

1. Proper settings in both CAMRAD II and CHARM must be used to produce the outputs required by AARON to complete acoustic predictions.
2. Use the 'reconstruction' option in CHARM and the 'post-trim' option in CAMRAD II to produce adequate azimuthal resolution for accurately capturing high-frequency acoustics. Additionally, use 50-100 aerodynamic panels in CHARM and 15-25 aerodynamic panels in CAMRAD II to obtain meaningful loading values. A panel study for the QSMR in forward flight with a free wake was conducted to verify the correct panel number settings.
3. Several variables are defined differently between CAMRAD II and CHARM and care must be taken to ensure correct modeling. The three settings considered in this section were: blade flapping, thrust coefficient, and number of revolutions.
4. When beginning to use either CAMRAD II or CHARM, it is important to begin with a simple rotor model and then increase complexity. For this work, a simple four-bladed rotor called the 'Lopes rotor' was used for this initial step. Then, to increase complexity, the three-bladed

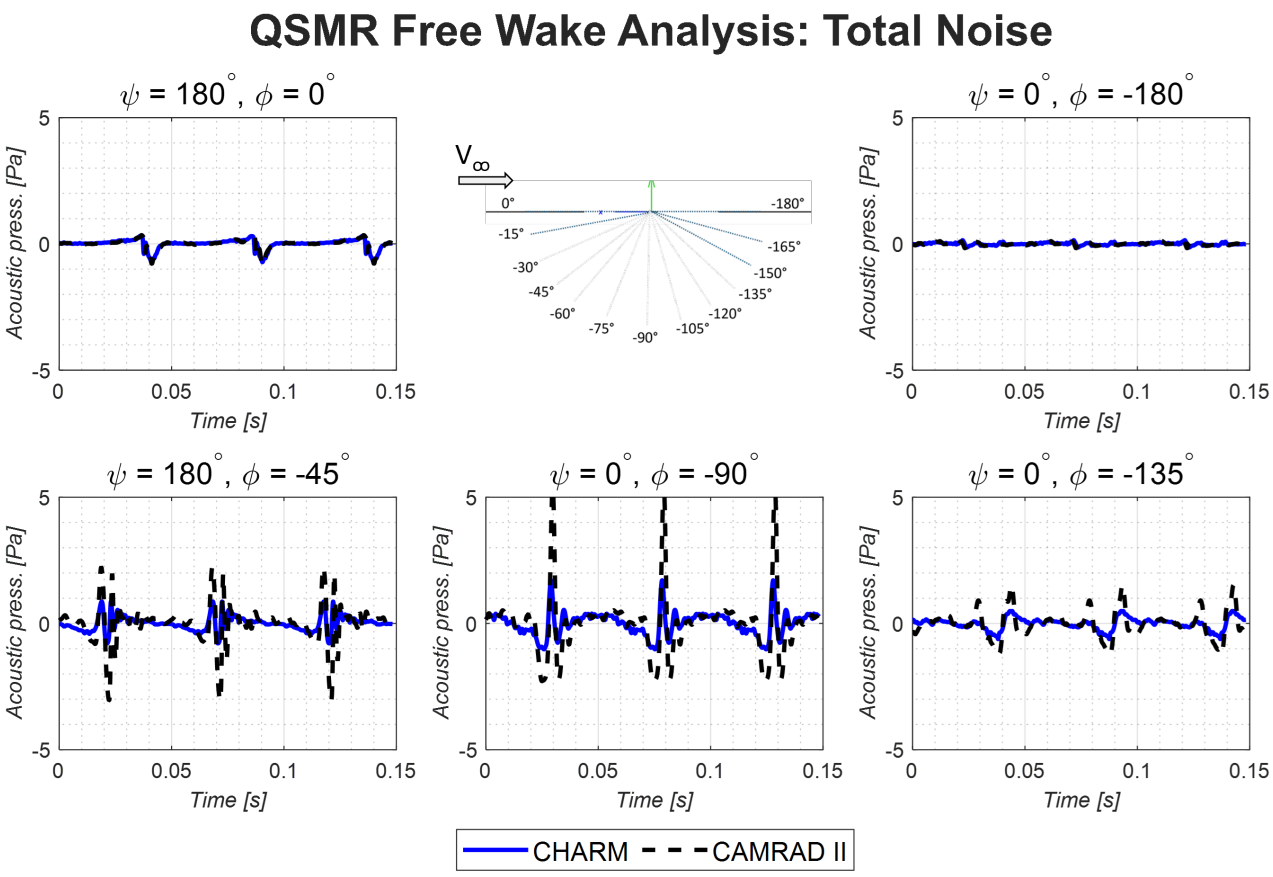

Figure 15. Total noise (thickness + loading) in CAMRAD II and CHARM using AARON for the QSMR in forward flight with a free wake model (V_{inf} =53.9 m/s, $\frac{C_T}{\sigma}$ = 0.07, μ = 0.25, α_s = -3°, θ_0 = 4°).

Quiet Single Main Rotor was used. Additionally, it is recommended to begin with hover and a 'simple wake' uniform inflow before moving on to more complicated cases. The 'simple wake' forward flight total tonal noise results for both the Lopes rotor and the QSMR for a selection of microphones were presented.

5. Both CAMRAD II and CHARM have different wake model options. This work recommends using increasing complexity to step through the wake models in order to ensure correct settings. The correct process of increasing wake complexity is simple wake to rigid wake to free wake.

6. The Brooks-Pope-Marcolini model used in AARON required specific airfoil inputs as well as outputs from the comprehensive codes. A BPM parametric study was conducted in order to identify and define these inputs and outputs to see their effect on broadband self-noise noise. Final broadband self-noise results for the Lopes rotor and QSMR with a free wake in forward flight were presented.

7. Metadata can be used to view plots of the internal calculations conducted by AARON. An example analysis of the vertical blade loading F_z for the QSMR in forward flight with a free wake for comparison between CAMRAD II and CHARM was shown.

8. The final free wake forward flight results for both the Lopes rotor and the QSMR for an array of 5 microphones were presented and discussed. For more simple rotors, good agreement between CAMRAD II and CHARM were found, while for more complex rotors, differences in the models leading to differences in loading noise were shown.

Although there will be additional settings for both CAMRAD II and CHARM for acoustic prediction that were not touched on in this paper, the current best practices do identify large areas of possible errors with the goal of providing a new user with the tools needed to use these codes for acoustic prediction. Future work entails extending these best practices to multirotors and full vehicle models.

Author contact:
Lauren Weist lauren.p.weist@nasa.gov
Natasha Schatzman natasha.schatzman@nasa.gov
Dorsa Shirazi dorsa.shirazi@nasa.gov

APPENDIX

Appendix A: Comprehensive analysis noise inputs

Figure 16 shows the input settings recommended to turn on acoustic outputs for CAMRAD II. This is required for using CAMRAD II to generate files that will be usable by AARON. If multiple rotors are being used, these settings need to be added for all rotors to output values for the entire configuration.

```
&NLDEF class='TRIM', &END
&NLVAL
       MPSIH  = 360,
       OPPOST =   1,
       ITERF  =   3,
&END
!============================================================
! ROTOR 1
!============================================================
&NLDEF class='TRIM ROTOR', name='ROTOR 1', &END
&NLVAL
       MHSEN = 1,  NHFILE = 1, MHTIME = 360,
       MCSEN = 1,  NCFILE = 1, MCTIME = 360,
       MBSEN = 1,  NBFILE = 1, MBTIME = 360,
       MPSEN = 1,  NPFILE = 1, MPTIME = 360,
       MASEN = 1,  NAFILE = 1, MATIME = 360,
&END
!------------------------------------------------------------
&NLDEF class='ROTOR', type='STRUCTURE', name='ROTOR 1', &END
&NLVAL
       OPSND = 1,
&END
!------------------------------------------------------------
&NLDEF class='ROTOR', type='AERODYNAMICS', name='ROTOR 1', &END
&NLVAL
       NSEN   =  7,
       QUANT  =  5,  5,  5, 53, 81, 81, 64,
       IDENT  =  0,  0,  0,  1,  1,  1,  1,
       AXIS   =  1,  2,  3,  0,  1,  3,  0,
       OPSCL  =  0,  0,  0,  1,  2,  2,  2,
       OPREF  =  1,  1,  1,  1,  2,  2,  2,
&END
!------------------------------------------------------------
&NLDEF class='ROTOR', type='WAKE', name='ROTOR 1', &END
&NLVAL
       OPFWG  = 3,
       CORE(1)= 0.8,
       OPTVIC = 0,
       OPRUDP = 0,
&END
```

Figure 16. Example input file of noise setting for CAMRAD II. Can be placed in a '.list' file.

Figure 17 depicts the input settings for CHARM in order to turn on acoustic outputs. These settings allow a user to generate the CHARM output files readable by AARON.

These are not all the settings required to produce accurate acoustic results, but instead the parameters needed to turn on the acoustic settings and produce results with adequate resolution.

Appendix B: Broadband self-noise parameter study

The baseline values for the BPM settings of the QSMR are presented in Table 3 as a fraction of total radius. The resolution is 0.05R up to and including the 0.85R radial location. These inputs were also used for the BPM settings for the QSMR model. BL_T is set to 0 for all radial stations, and is therefore not included in the table.

```
IRECON    NOISE     KBROADBAND KSEL
 1         -4        1          1
ACOUSTICS_CODE
 2
NCHDRC    NPSIRC    IVROLL     CDRMIN     IRECONTYPE
 1         360       1          0.02       1
```

Figure 17. Example input file of noise setting for CHARM. These settings are located in the main '.inp' file.

Table 3. QSMR BPM parameter study baseline (Case 1).

r/R	Airfoil	t/c	α_0	h	θ_{TE}
0.00	VR-12	0.106	-1.470	0.0021	14.31
0.05	VR-12	0.106	-1.470	0.0021	14.31
0.10	VR-12	0.106	-1.470	0.0021	14.31
0.15	VR-12	0.106	-1.470	0.0021	14.31
0.20	VR-12	0.106	-1.470	0.0021	14.31
0.25	VR-12	0.106	-1.470	0.0021	14.31
0.30	VR-12	0.106	-1.470	0.0021	14.31
0.35	VR-12	0.106	-1.470	0.0021	14.31
0.40	VR-12	0.106	-1.470	0.0021	14.31
0.45	VR-12	0.106	-1.470	0.0021	14.31
0.50	VR-12	0.106	-1.470	0.0021	14.31
0.55	VR-12	0.106	-1.477	0.0021	14.31
0.60	VR-12	0.106	-1.482	0.0021	14.31
0.65	VR-12	0.106	-1.488	0.0021	14.31
0.70	VR-12	0.106	-1.492	0.0021	14.31
0.75	VR-12	0.106	-1.492	0.0021	14.31
0.80	VR-12	0.106	-1.487	0.0021	14.31
0.85	VR-12	0.106	-1.505	0.0021	14.31
0.94	SSC-A09	0.09	-1.048	0.0023	8.16
1.00	SSC-A09	0.09	-1.013	0.0023	8.16

ACKNOWLEDGMENTS

Special thanks to Wayne Johnson, Doug Boyd, Leonard Lopes, and Chris Silva, who are always willing to answer our questions and helped us work through learning these codes. Their guidance and expertise has been immeasurably helpful.

Funding for this effort was provided by the NASA Revolutionary Vertical Lift Technology Project.

REFERENCES

1. Johnson, W., "CAMRAD II Comprehensive Analytical Model of Rotorcraft Aerodynamics and Dynamics," Johnson Aeronautics, Palo Alto, CA, 2005.

2. Wachspress, D.A., Quackenbush, T.R., and Boschitsch, A.H., "Rotorcraft Interactional Aerodynamics with Fast

Vortex/Fast Panel Methods," *Journal of the American Helicopter Society*, Volume 48, Number 4, 1 October 2003, pp. 223-235(13).

3. Lopes, L. V. and Burley, C. L., "ANOPP2 User's Manual: Version 1.2," NASA/TM-2016-219342, October 2016.

4. Lopes, L. V., "Compact Assumption Applied to Monopole Term of Farassat's Formulations," *Journal of Aircraft*, Vol. 54, No. 5, September-October 2017, p. 1649–1663.

5. Johnson, W., "A Quiet Helicopter for Air Taxi Operations," Vertical Flight Society Aeromechanics for Advanced Vertical Flight Technical Meeting, San Jose, CA, January 2020.

6. Silva, C. and Johnson, W., "Practical Conceptual Design of Quieter Urban VTOL Aircraft," Vertical Flight Society 77th Annual Forum, Online, May 2021.

7. Farassat, F., "Derivation of Formulations 1 and 1A of Farassat," NASA/TM-2007-214853, March 2007.

8. Brooks, T. F., Pope, D. S. and Marcolini, M. A., "Airfoil Self-Noise and Prediction," NASA RP 1218, July 1989.

9. Meyn, L., "Rotorcraft Optimization Tools: Incorporating Rotorcraft Design Codes into Multi-Disciplinary Design, Analysis, and Optimization," AHS Technical Meeting on Aeromechanics Design for Vertical Lift, San Francisco, CA, January 2018.

10. Johnson, W., "A General Free Wake Geometry Calculation for Wings and Rotors," American Helicopter Society 51st Annual Forum, Fort Worth, TX, May 1995.

11. Kottapalli, S., Silva, C., and Boyd, D., "Effect of Rotor Blade Elasticity on UAM Quadrotor Acoustics," Presented at the Vertical Flight Society 79th Annual Forum Technology Display, West Palm Beach, FL, May 2023.

12. Kottapalli, S. and Silva, C., "Prediction of Quadrotor Acoustics Using RVLT Toolchain," Presented at the VFS Aeromechanics for Advanced Vertical Flight Technical Meeting, San Jose, CA, Jan 2022.

13. Weist, L. and Schatzman, N., "RABBIT: A Rapid Low Fidelity BVI Prediction Tool—Comparison and Validation using the NASA RVLT Toolchain," Presented at the VFS Aeromechanics for Advanced Vertical Flight Technical Meeting, San Jose, CA, Jan 2022.